Realistic ice-shelf/ocean state estimates (RISE) of basal melting and drivers: supplementary material

Benjamin K. Galton-Fenzi[1,2,3], Richard Porter-Smith[1,2], Sue Cook[2], Eva Cougnon[4], David E. Gwyther[5], Wilma G. C. Huneke[6], Madelaine G. Rosevear[7,3], Xylar Asay-Davis[8], Fabio Boeira Dias[9,3], Michael S. Dinniman[10], David Holland[11], Kazuya Kusahara[12], Kaitlin A. Naughten[13], Keith W. Nicholls[13], Charles Pelletier[14], Ole Richter[15,16], Hélène Seroussi[17], and Ralph Timmermann[16]

[1]Australian Antarctic Division, Kingston, Tasmania, Australia
[2]Australian Antarctic Program Partnership, Institute for Marine and Antarctic Studies, University of Tasmania, Australia
[3]Australian Centre for Excellence in Antarctic Science, University of Tasmania, Australia
[4]Integrated Marine Observing System, Hobart, Tasmania
[5]University of Queensland, Australia
[6]Australian Centre of Excellence for Climate Extremes, Australian National University, Canberra, Australia
[7]Melbourne University, Australia
[8]Los Alamos National Laboratory, USA
[9]University of New South Wales, Australia
[10]Old Dominion University, Virginia, USA
[11]New York University, USA
[12]Japan Agency for Marine-Earth Science and Technology, Japan
[13]British Antarctic Survey, Cambridge, UK
[14]Earth and Life Institute (ELI), UCLouvain, Louvain-la-Neuve, Belgium
[15]University of Rostock, Germany
[16]Alfred Wagner Institute, Germany
[17]Dartmouth College, New Hampshire, USA

Correspondence: Benjamin K. Galton-Fenzi (ben.galton-fenzi@aad.gov.au)

S1 Model setup

Table S1. Further details of the models used in this study. Details for each model can be found in the corresponding primary reference for each model supplied in the main text.

Identifier	Domain	Atmosphere forcing	Sea ice	Ice shelf geometry	Vertical coordinate	Surface resolution	Ice shelf frazil	Ice shelf fluxes
COCO	Global	ERA-Interim[1]	2-layer	RTopo-2[2]	z [4]	5 m	no	uppermost
DINN	Regional	ERA-Interim	Budgell	RTopo-2[3]	s	variable	yes	uppermost
E302	Global	Fully coupled[4]	MPAS-SI	Bedmap2[5]	$z^\star$ [6]	variable[6]	no	distributed[7]
FESH	Global	ERA-Interim	2-layer	RTopo-1.05[8]	z-σ [9]	variable[9]	no	uppermost
FESL	Global	ERA-Interim	2-layer	RTopo-1.05	z-σ [9]	variable[9]	no	uppermost
METR	Regional	ERA-Interim	CICE	RTopo-1.05	s	variable	yes	uppermost
NE01	Global	COSMO-CLM	LIM	Bedmachine[10]	$z^\star$ [1]	variable	no	distributed[11]
NE02	Global	COSMO-CLM	LIM	Bedmachine[12]	$z^\star$ [1]	variable	no	distributed[11]
RICH	Regional	ERA-Interim[13]	Prescribed[13]	Bedmap2/RTopo-2[14]	s	variable	no	uppermost

[1] Dee et al. (2011).

[2] Schaffer et al. (2016).

[3] Including updates for the Amundsen Sea Embayment (Millan et al., 2017).

[4] partial step following Losch (2008).

[4] The 150 years are taken from a coupled atmosphere-ocean-sea-ice-land preindustrial simulation (repeat 1850).

[5] Fretwell et al. (2013).

[6] With adjustments for the top layer to follow the ice draft.

[7] Driving fluxes are the average, and meltwater production is distributed vertically, over the upper 10 m following Gwyther et al. (2020).

[8] Timmermann et al. (2010).

[9] 22 layer σ (equally spaced) coordinate under ice shelves.

[10] Morlighem et al. (2020).

[11] Estimated by calculating the driving fluxes as a mean over the upper 10 m, as with [5] (Mathiot et al., 2017).

[12] Bedmachine data was interpolated to the ice sheet model domain derived from the initialization and relaxation procedure of f.ETISh (Pelletier et al., 2022).

[13] Sea ice fluxes are prescribed, combining atmospheric reanalysis with satellite estimates of sea ice production (Tamura et al., 2011).

[14] Blended product including several local and regional modifications.

S2 Methods

S2.1 Examples of Veronni tessellation

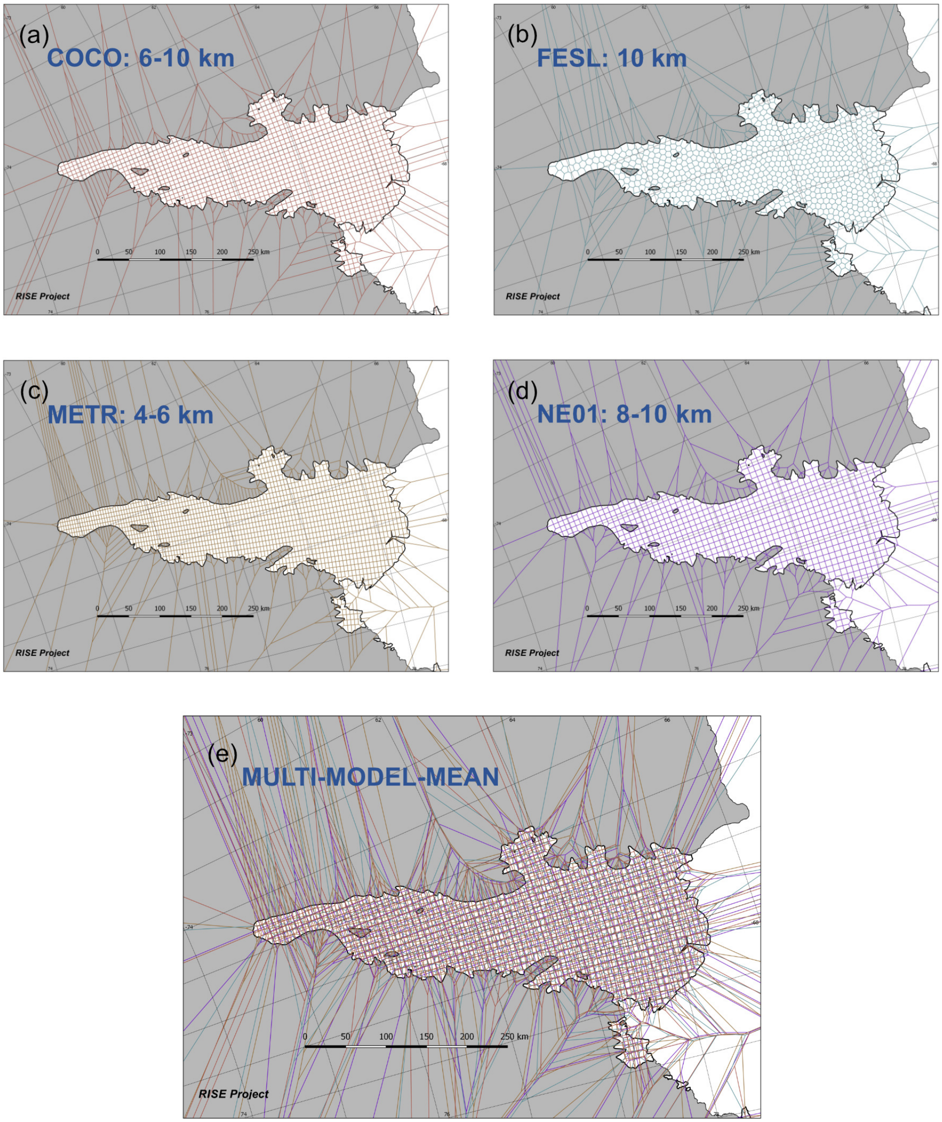

Figure S1. Examples of the Veronni tessellation for the Amery Ice Shelf, used for 4 different models and associated different horizontal resolutions and native mesh type, and how they overlap to produce the Multi-Model Mean for a) COCO, b) FESL, c) METR, d) NE01 and e) MMM.

S3 Comparison with satellite observations

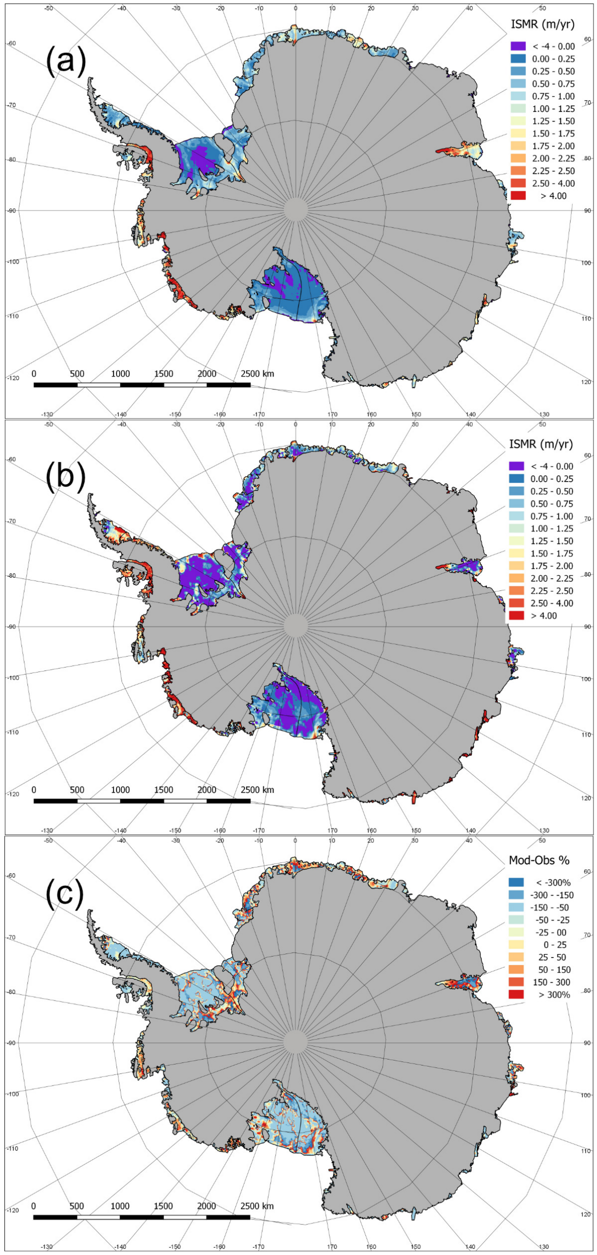

Figure S2. Comparison of melt rates between a) the Multi-model Mean (MMM) and b) Satellite based estimates (SATT). c) is the percentage difference between MMM and SATT, calculated as (MMM - SATT)/ SATT)$\times$100

S4 Individual Ice Shelf examples

S4.1 Amery Ice Shelf

Table S2. Amery Ice Shelf, East Antarctica

Identifier	Cavity Volume (km^3)	Melt rate (m $year^{-1}$)	Mass loss (Gt $year^{-1}$) Net	Melt	Freeze	Freeze/Melt $\times 100$ (%)
MMM	28885	1.54	85.59	86.24	0.64	0.74
COCO	29682	0.78	43.59	45.26	1.67	3.69
DINN	27981	0.40	22.34	24.95	2.61	10.46
E302	34595	4.16	231.88	231.88	0.00	0.00
FESH	38125	1.17	65.38	71.45	6.07	8.50
FESL	38959	1.23	68.67	73.84	5.17	7.00
METR	32806	1.43	79.60	80.48	0.88	1.09
NE01	30631	3.00	167.41	167.47	0.06	0.04
NE02	29990	1.45	80.71	80.72	0.01	0.01
RICH	23634	0.19	10.77	16.90	6.13	36.27
SATT	-	0.90	49.59	61.17	11.58	18.93

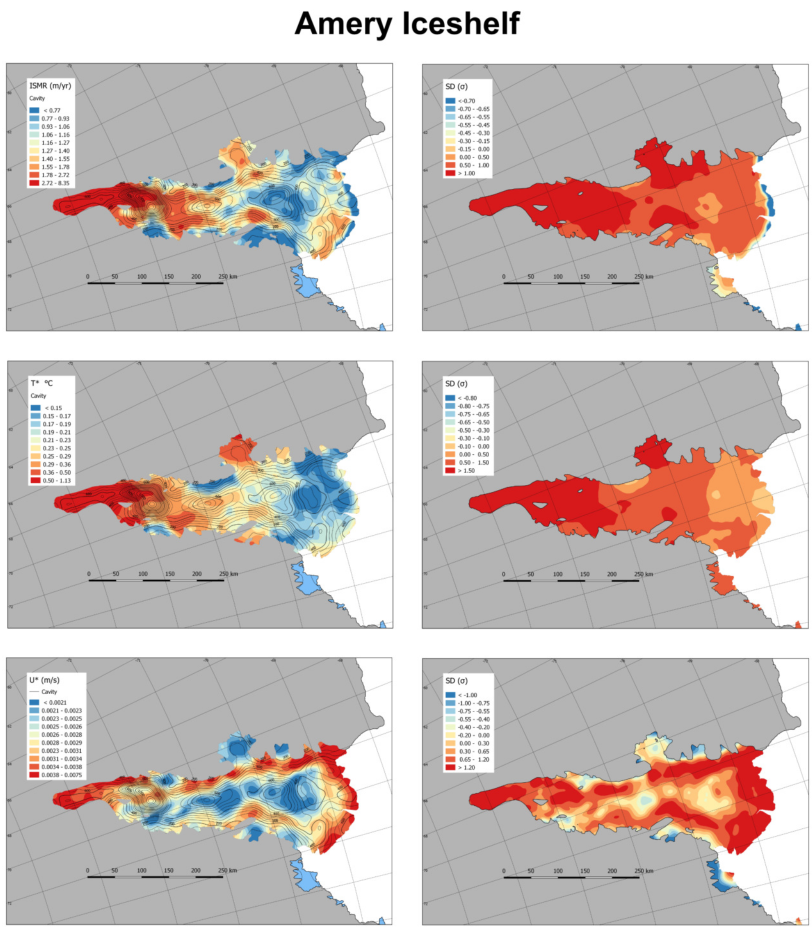

Figure S3. Maps of the Amery Ice Shelf, East Antarctica, for the Multi-Model Mean, of the ice shelf melt rate (ISMR, top-left), $T^\star$ (middle-left), $u^\star$ (bottom-left) and their corresponding standard deviation across the models (right-hand panels).

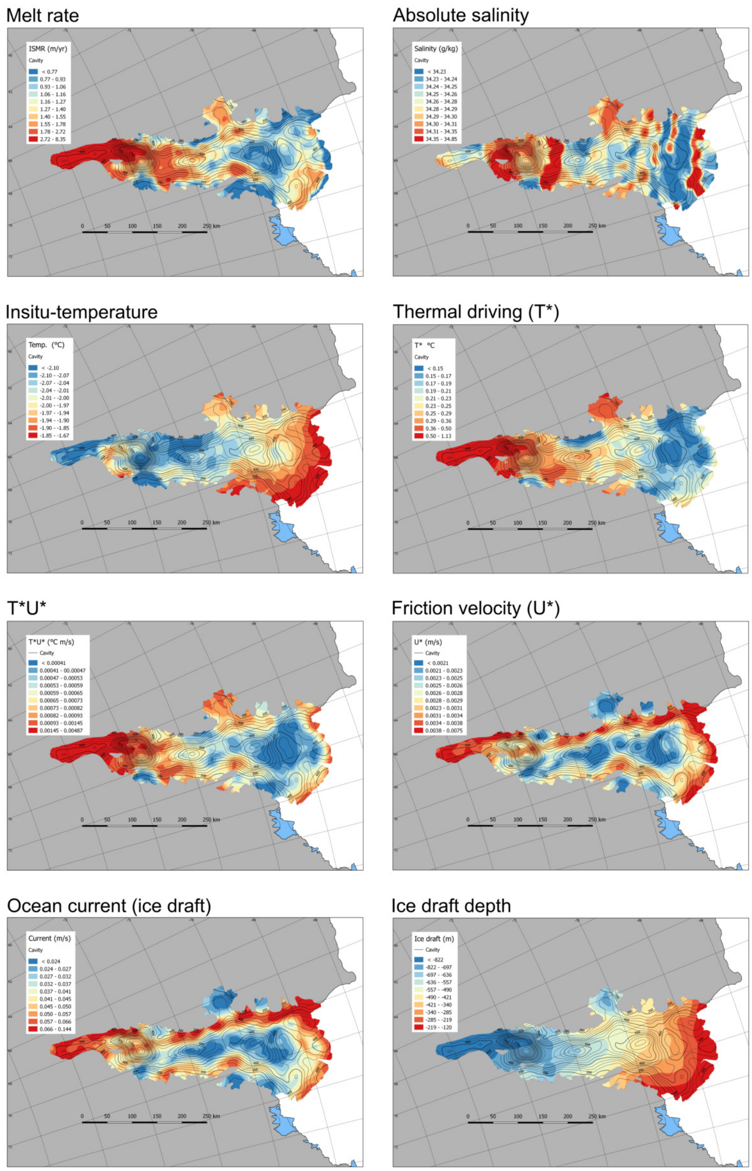

Figure S4. Maps of the Amery Ice Shelf, East Antarctica, for the Multi-Model Mean.

S4.2 Fimbul Ice Shelf

Table S3. Fimbul Ice Shelf, East Antarctica

Identifier	Cavity Volume (km^3)	Melt rate (m $year^{-1}$)	Mass loss (Gt $year^{-1}$) Net	Melt	Freeze	Freeze/Melt $\times$100 (%)
MMM	19259	0.94	35.43	35.55	0.12	0.34
COCO	48129	1.93	72.38	72.38	0.00	0.00
DINN	48290	1.18	44.16	44.60	0.44	0.99
E302	49838	0.83	31.34	31.34	0.00	0.00
FESH	46832	0.99	37.09	43.19	6.10	14.12
FESL	48742	0.84	31.47	35.45	3.97	11.20
METR	39290	0.55	20.56	20.57	0.01	0.05
NE01	45447	0.40	14.87	14.88	0.01	0.07
NE02	45806	0.34	12.88	12.88	0.00	0.00
RICH	47907	1.44	54.12	54.18	0.06	0.11
SATT	-	0.88	32.81	35.64	2.82	7.91

Fimbul Iceshelf

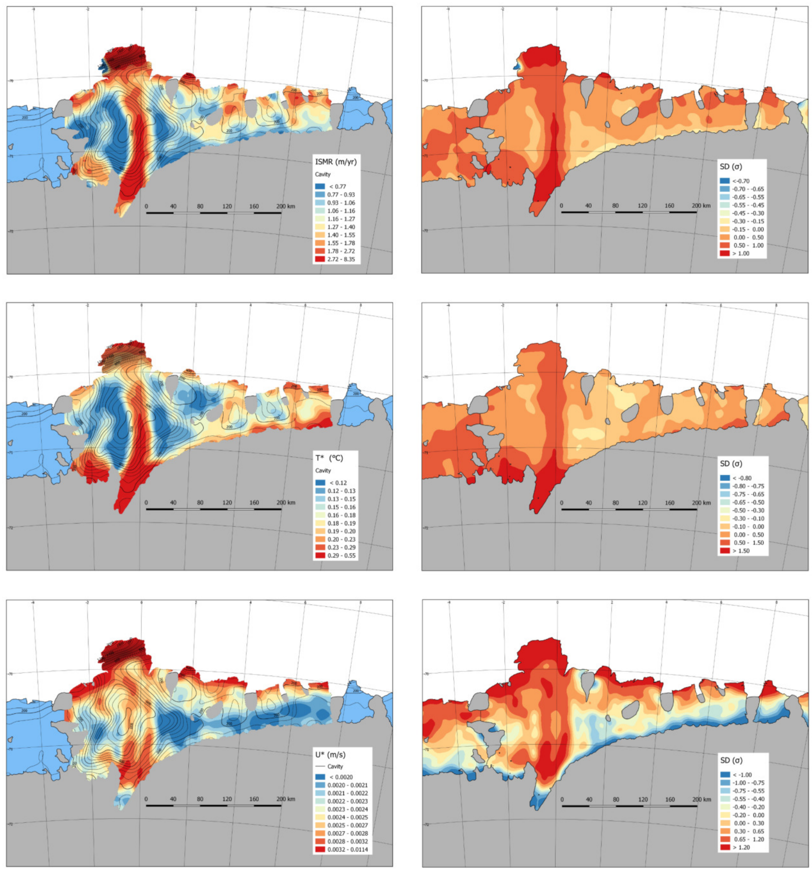

Figure S5. Maps of the Fimbul Ice Shelf, East Antarctica, for the Multi-Model Mean, of the ice shelf melt rate (ISMR, top-left), $T^{\star}$ (middle-left), $u^{\star}$ (bottom-left) and their corresponding standard deviation across the models (right-hand panels).

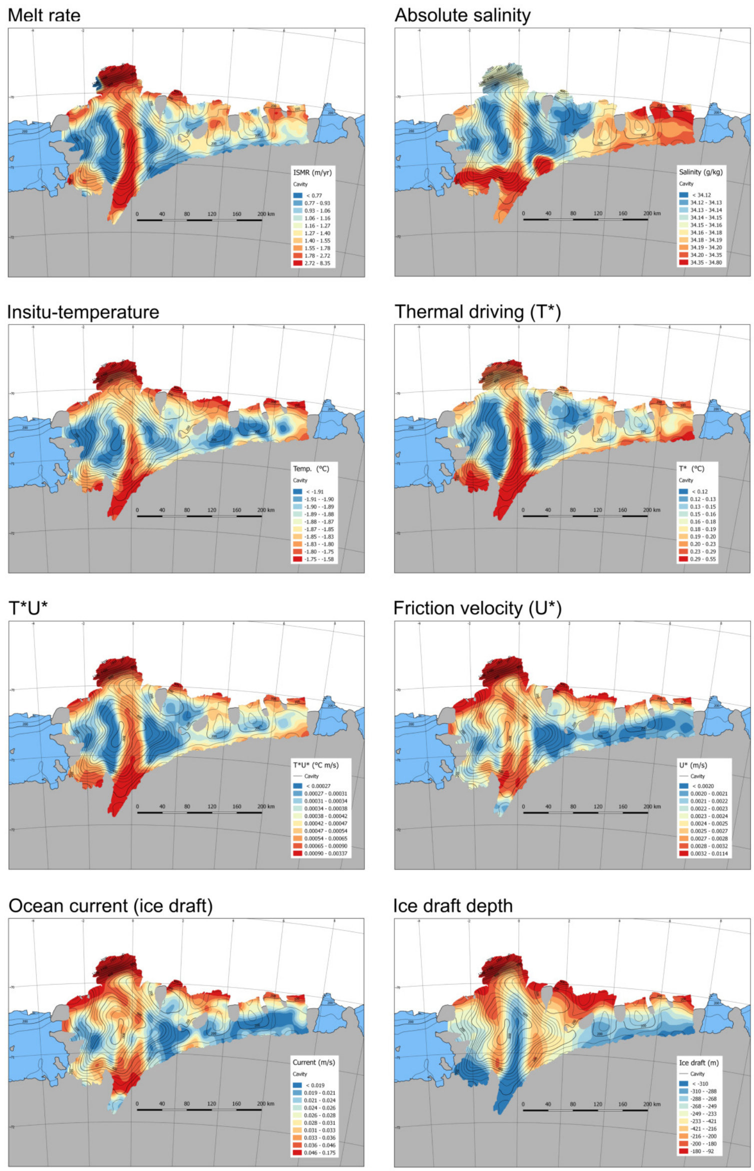

Figure S6. Maps of the Fimbul Ice Shelf, East Antarctica, for the Multi-Model Mean.

S4.3 Larsen Ice Shelf

Table S4. Larsen C, Antarctic Peninsula

Identifier	Cavity Volume (km^3)	Melt rate (m $year^{-1}$)	Mass loss (Gt $year^{-1}$) Net	Melt	Freeze	Freeze/Melt $\times$100 (%)
MMM	13378	0.59	25.56	25.59	0.03	0.12
COCO	22027	0.54	23.54	23.59	0.05	0.21
DINN	20996	0.34	14.71	15.04	0.33	2.19
E302	22624	0.65	28.35	28.35	0.00	0.00
FESH	23407	1.23	53.47	55.11	1.63	2.96
FESL	24716	0.83	36.14	38.86	2.72	7.00
METR	21585	0.39	16.97	16.97	0.00	0.00
NE01	19577	0.60	26.00	26.03	0.02	0.08
NE02	20497	0.49	21.50	21.51	0.01	0.05
RICH	18183	0.22	9.37	10.48	1.10	10.50
SATT	-	1.67	65.31	66.19	0.87	1.31

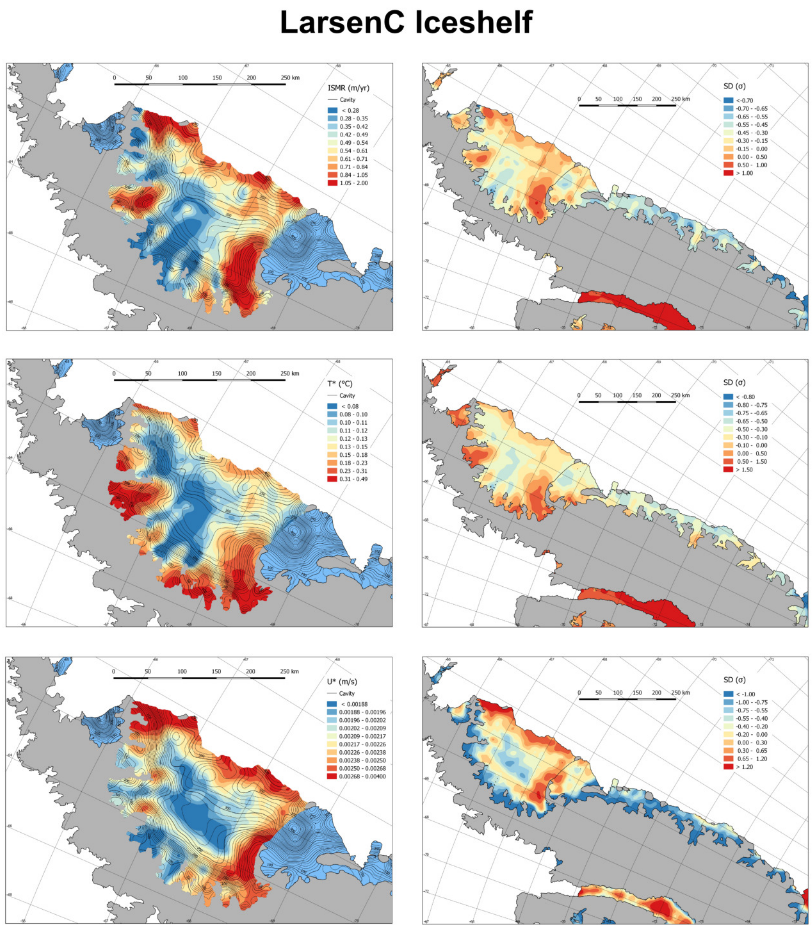

Figure S7. Maps of the Larsen C Ice Shelf, Antarctic Peninsula, for the Multi-Model Mean, of the ice shelf melt rate (ISMR, top-left), $T^{\star}$ (middle-left), $u^{\star}$ (bottom-left) and their corresponding standard deviation across the models (right-hand panels).

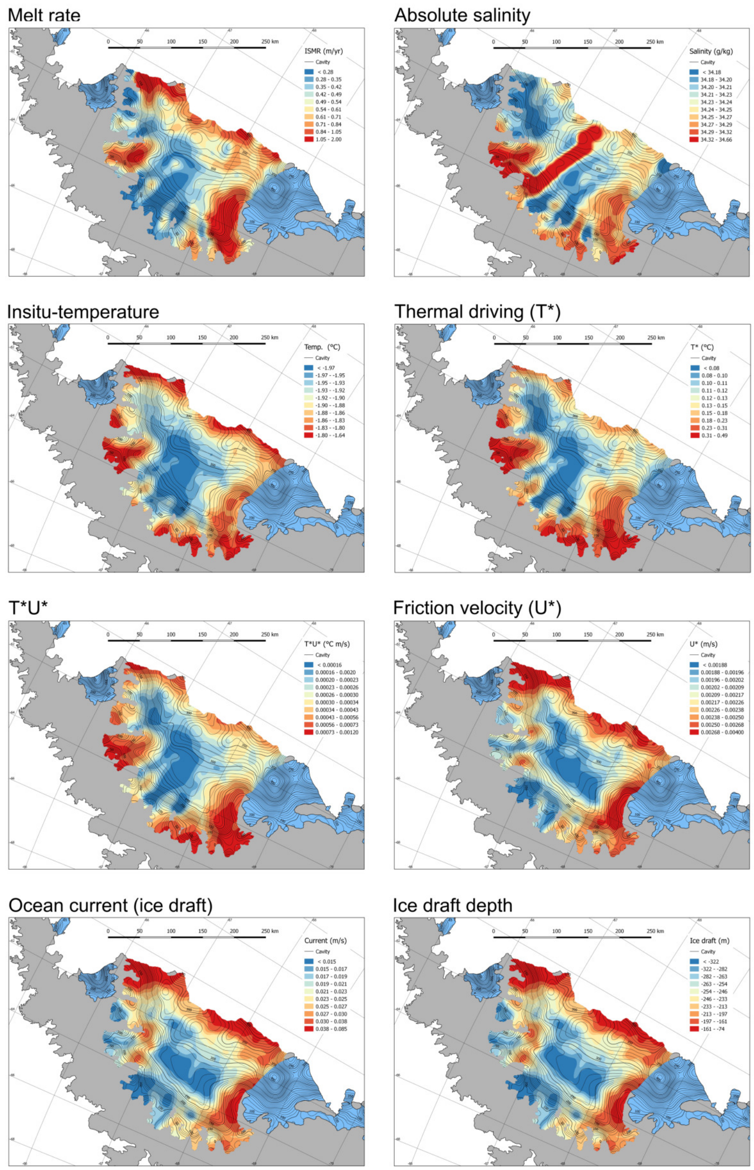

Figure S8. Maps of the Larsen C Ice Shelf, Antarctic Peninsula, for the Multi-Model Mean.

S4.4 Ronne-Filchner Ice Shelf, East Antarctica

Table S5. Ronne-Filchner Ice Shelf, East Antarctica

Identifier	Cavity Volume (km^3)	Melt rate (m $year^{-1}$)	Mass loss (Gt $year^{-1}$) Net	Melt	Freeze	Freeze/Melt ×100 (%)
MMM	139388	0.21	62.95	75.26	12.31	16.36
COCO	160448	0.23	69.39	94.42	25.03	26.51
DINN	153642	0.09	25.76	64.00	38.24	59.75
E302	167984	0.30	91.18	93.37	2.18	2.33
FESH	152412	0.17	50.02	58.20	8.18	14.05
FESL	160461	0.16	47.29	55.55	8.26	14.87
METR	143434	0.10	29.38	39.91	10.53	26.38
NE01	133179	0.32	97.35	126.98	29.63	23.33
NE02	131269	0.24	73.08	94.95	21.87	23.03
RICH	130002	0.28	83.11	103.98	20.88	20.08
SATT	-	0.07	21.76	120.83	99.06	81.98

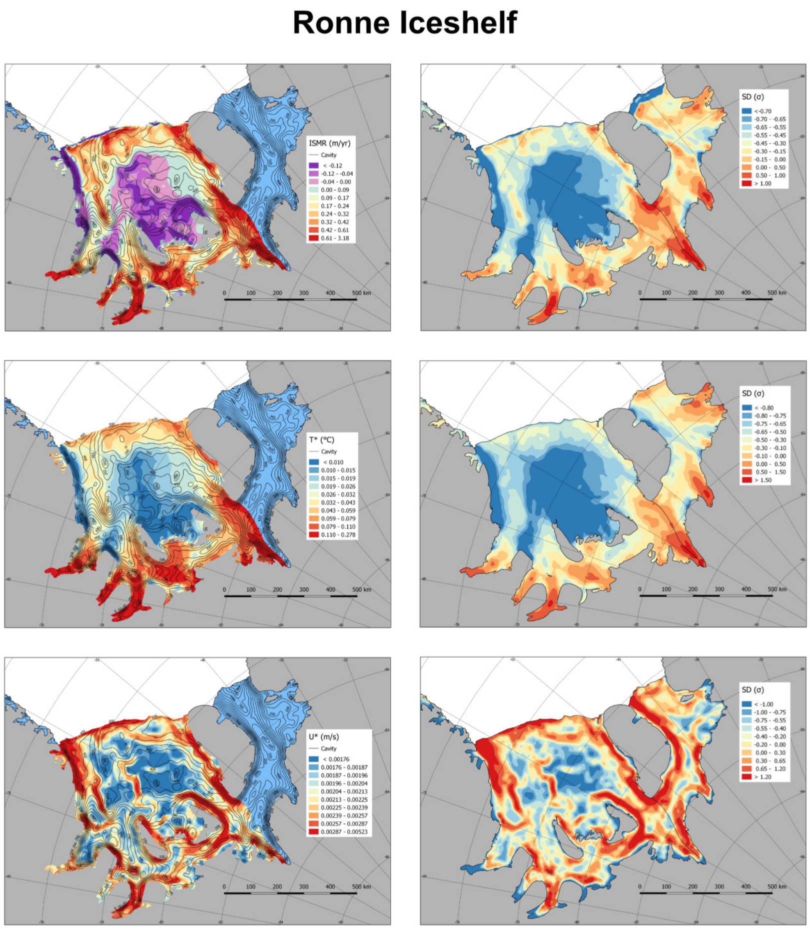

Figure S9. Maps of the Ronne-Filchner Ice Shelf, East Antarctica, for the Multi-Model Mean, of the ice shelf melt rate (ISMR, top-left), $T^\star$ (middle-left), $u^\star$ (bottom-left) and their corresponding standard deviation across the models (right-hand panels).

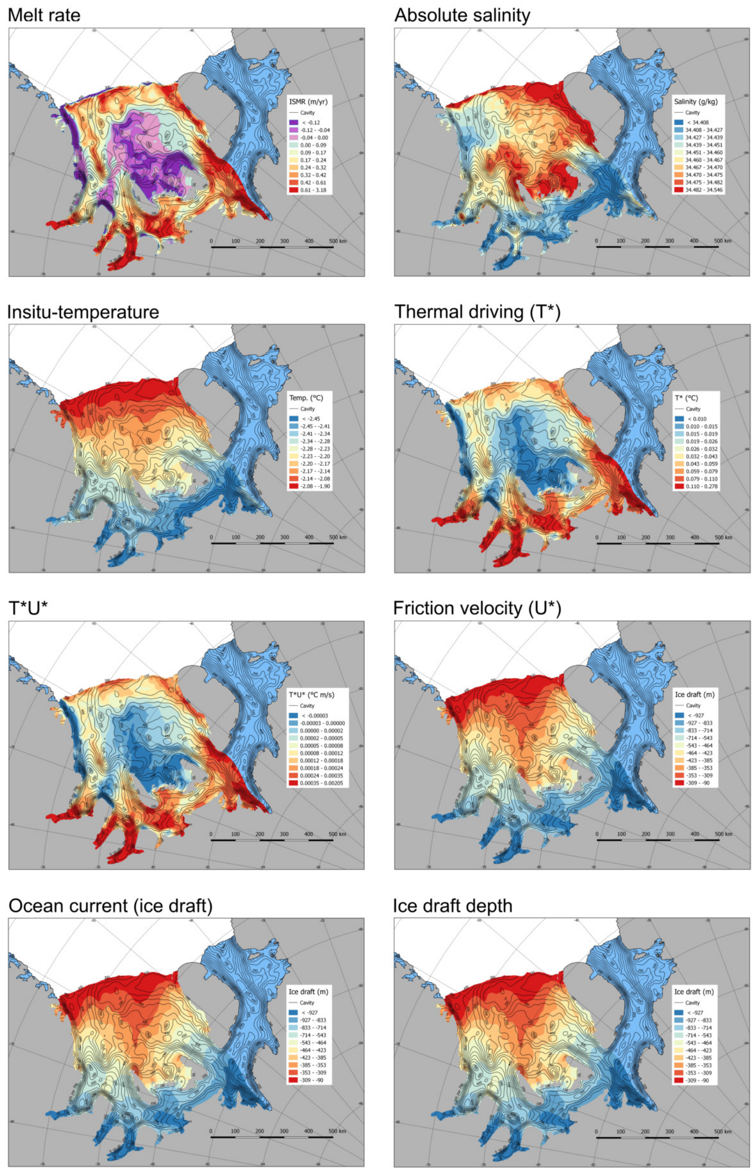

Figure S10. Maps of the Ronne-Filchner Ice Shelf, East Antarctica, for the Multi-Model Mean.

S4.5 Ross Ice Shelf, West Antarctica

Table S6. Ross Ice Shelf, West Antarctica

Identifier	Cavity Volume (km^3)	Melt rate (m $year^{-1}$)	Mass loss (Gt $year^{-1}$)			Freeze/Melt
			Net	Melt	Freeze	$\times$100 (%)
MMM	211298	0.16	78.23	68.31	9.94	14.55
COCO	245992	0.26	122.97	113.94	9.03	7.93
DINN	235836	0.11	70.94	49.42	21.52	43.55
E302	236100	0.15	69.05	67.60	1.45	2.14
FESH	244455	0.16	117.82	69.18	48.63	70.29
FESL	253107	0.15	100.72	67.07	33.65	50.17
METR	237892	0.13	60.03	57.72	2.31	4.00
NE01	218505	0.15	74.02	67.46	6.56	9.72
NE02	217227	0.13	59.95	57.98	1.97	3.40
RICH	225819	0.15	71.35	64.33	7.01	10.90
SATT	-	0.13	113.93	58.24	55.69	95.62

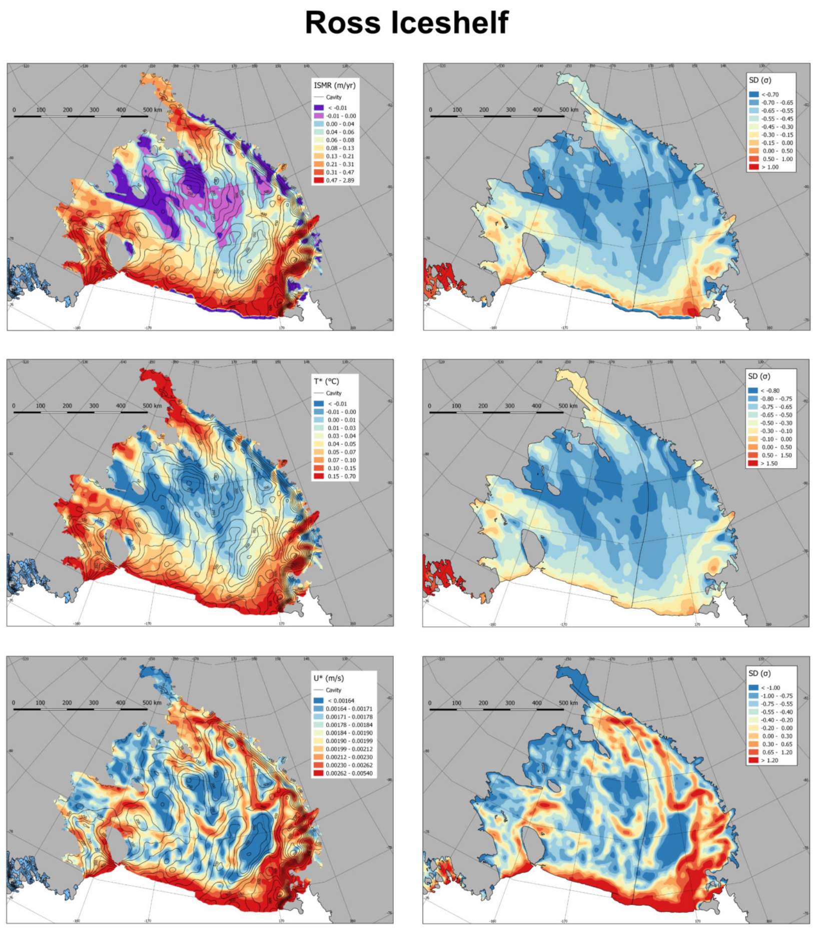

Figure S11. Maps of the Ross Ice Shelf, West Antarctica, for the Multi-Model Mean, of the ice shelf melt rate (ISMR, top-left), $T^{\star}$ (middle-left), $u^{\star}$ (bottom-left) and their corresponding standard deviation across the models (right-hand panels).

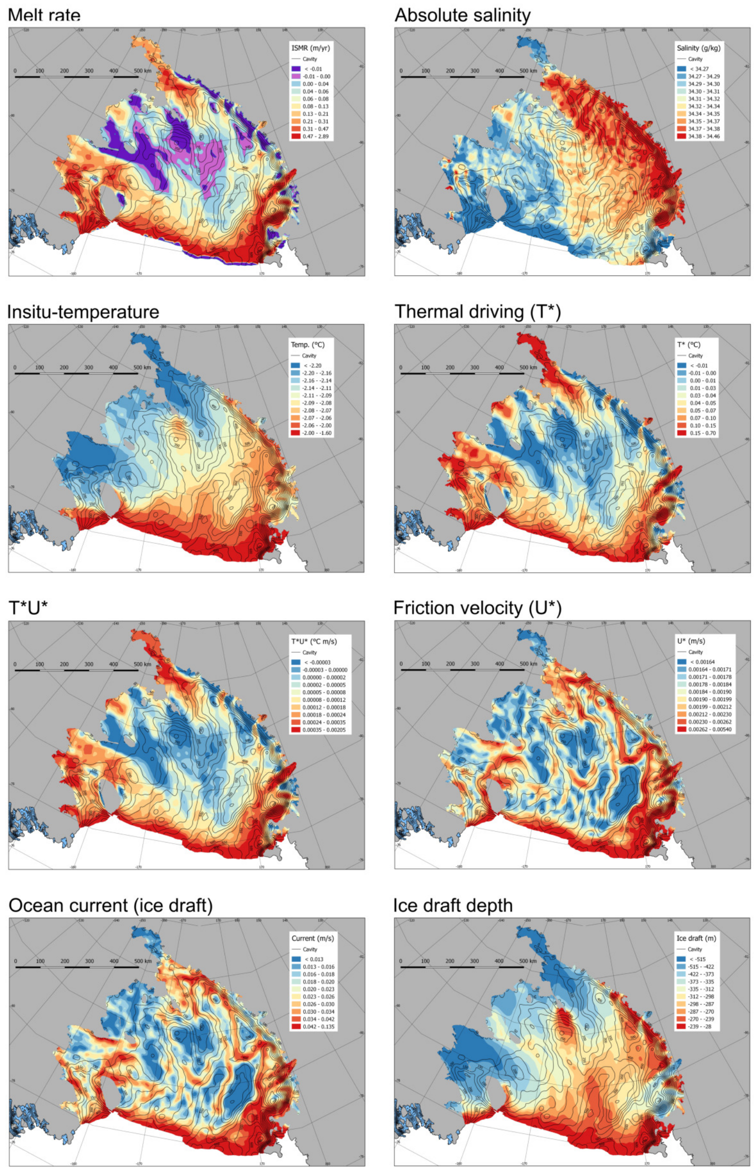

Figure S12. Maps of the Ross Ice Shelf, West Antarctica, for the Multi-Model Mean.

S4.6 Thwaites Ice Shelf, West Antarctica

Table S7. Thwaites Ice Shelf, West Antarctica

Identifier	Cavity Volume (km^3)	Melt rate (m $year^{-1}$)	Mass loss (Gt $year^{-1}$) Net	Melt	Freeze	Freeze/Melt $\times$100 (%)
MMM	3332	3.04	14.99	15.53	0.54	3.48
COCO	4762	1.42	6.99	6.99	0.00	0.00
DINN	4352	4.57	22.54	23.29	0.75	3.22
E302	5226	1.17	5.78	5.78	0.00	0.00
FESH	5353	0.30	1.48	6.60	5.12	77.58
FESL	5732	0.10	0.51	3.57	3.07	85.99
METR	4537	1.58	7.81	7.81	0.00	0.00
NE01	4925	3.77	18.56	18.56	0.00	0.00
NE02	5099	8.17	40.28	40.28	0.00	0.00
RICH	3623	6.28	30.96	30.97	0.02	0.06
SATT	-	29.71	81.04	81.05	0.00	0.00

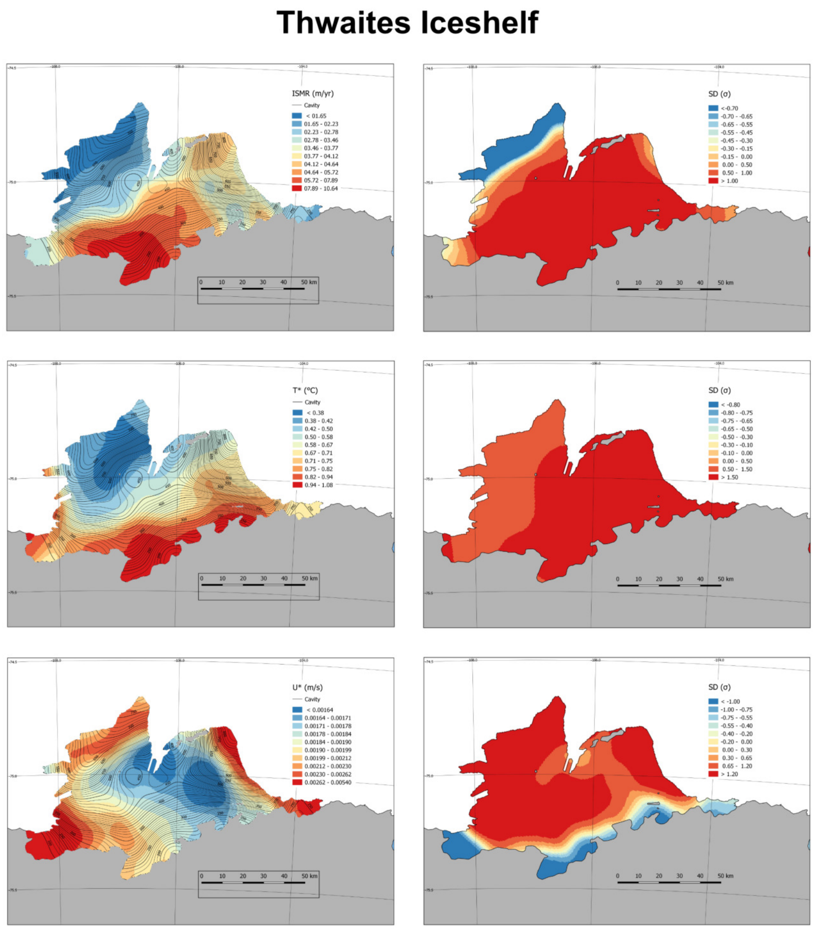

Figure S13. Maps of the Thwaites Ice Shelf, West Antarctica, for the Multi-Model Mean, of the ice shelf melt rate (ISMR, top-left), $T^{\star}$ (middle-left), $u^{\star}$ (bottom-left) and their corresponding standard deviation across the models (right-hand panels).

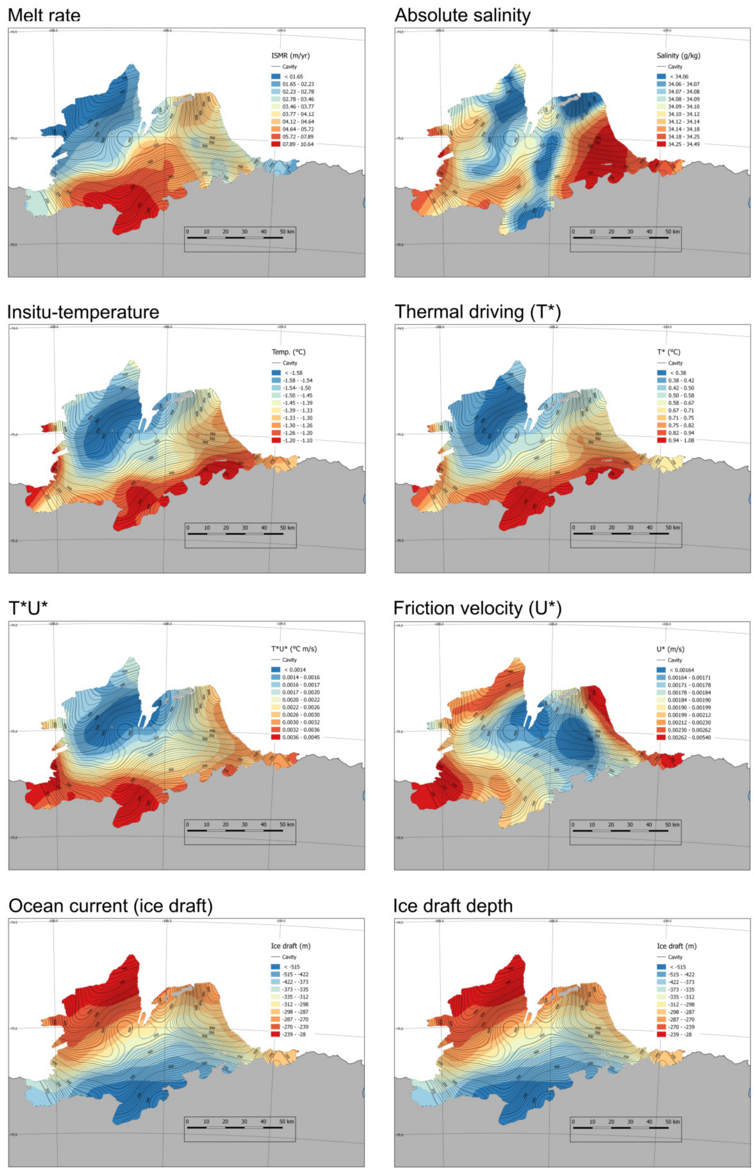

Figure S14. Maps of the Thwaites Ice Shelf, West Antarctica, for the Multi-Model Mean.

S4.7 Totten Ice Shelf, East Antarctica.

Table S8. Totten Ice Shelf, East Antarctica

Identifier	Cavity Volume (km^3)	Melt rate (m $year^{-1}$)	Mass loss (Gt $year^{-1}$) Net	Melt	Freeze	Freeze/Melt $\times$100 (%)
MMM	2292	2.23	12.63	12.64	0.01	0.08
COCO	2282	1.50	8.52	8.52	0.00	0.00
DINN	1367	0.43	2.45	2.54	0.10	3.94
E302	4316	2.69	15.27	15.27	0.00	0.00
FESH	2433	1.31	7.43	7.73	0.30	3.88
FESL	3044	0.79	4.50	4.59	0.10	2.18
METR	1076	0.71	4.05	4.05	0.00	0.00
NE01	3886	5.37	30.46	30.46	0.00	0.00
NE02	3439	6.00	34.04	34.04	0.00	0.00
RICH	499	1.23	6.98	8.06	1.07	13.28
SATT	-	10.65	59.39	60.04	0.65	-1.08

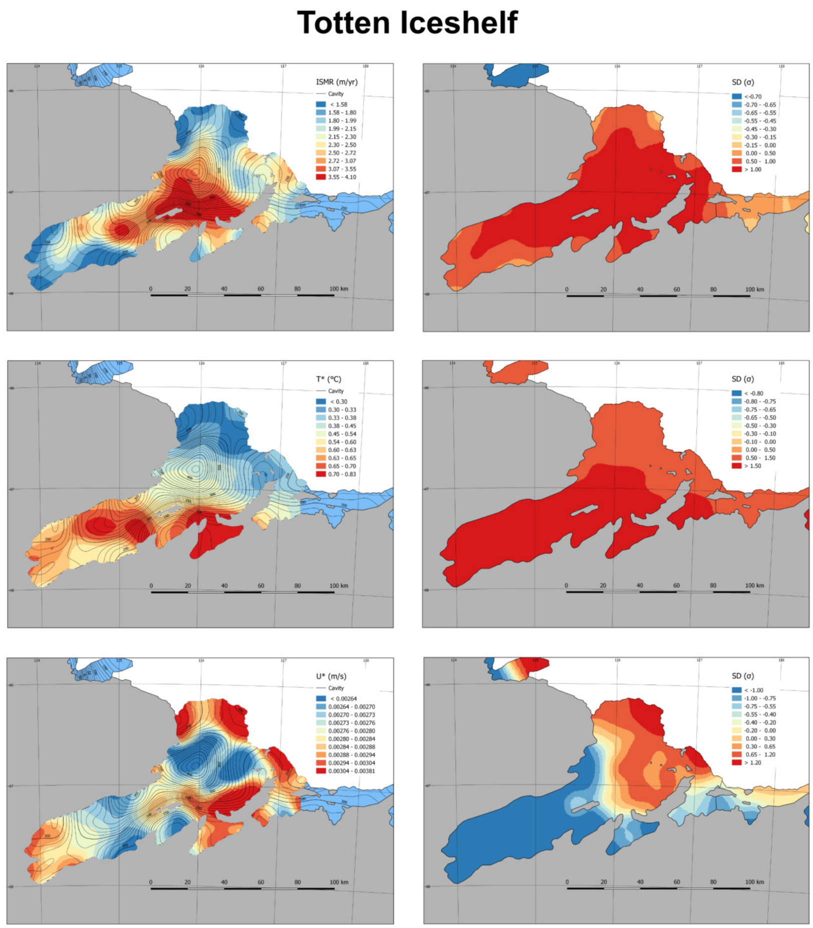

Figure S15. Maps of the Totten Ice Shelf, East Antarctica, for the Multi-Model Mean, of the ice shelf melt rate (ISMR, top-left), $T^{\star}$ (middle-left), $u^{\star}$ (bottom-left) and their corresponding standard deviation across the models (right-hand panels).

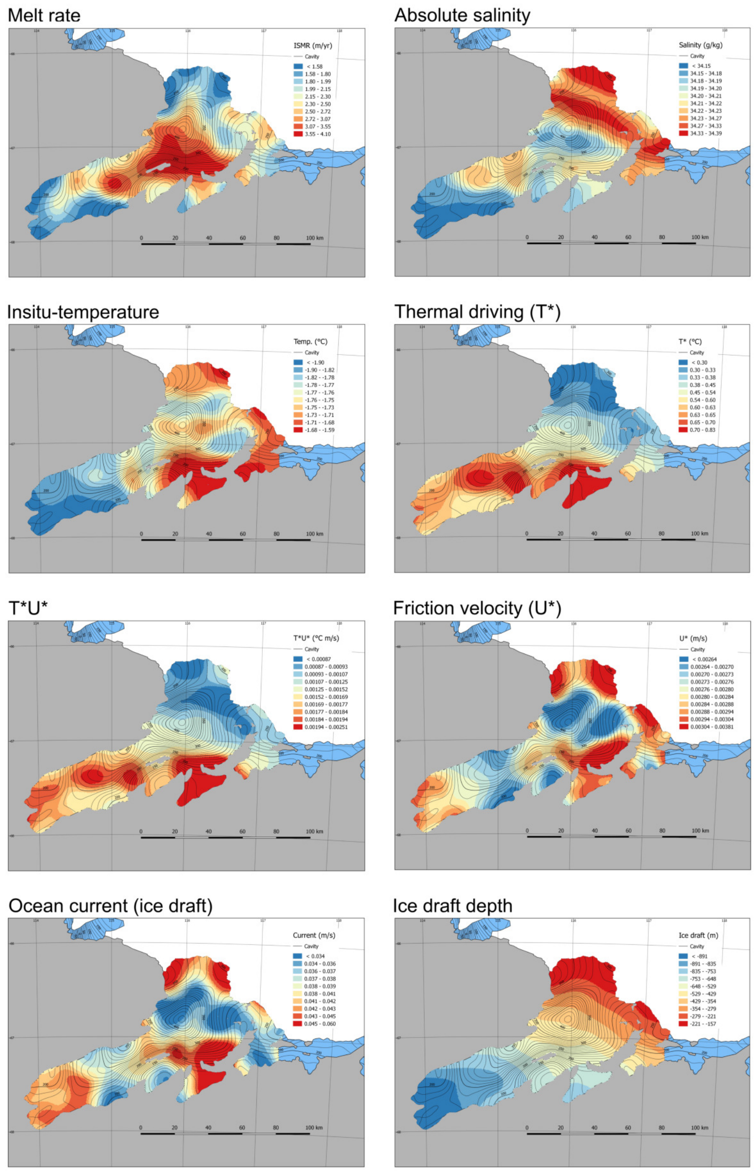

Figure S16. Maps of the Totten Ice Shelf, East Antarctica, for the Multi-Model Mean.

S5 Comparison of contributing model results for Antarctica

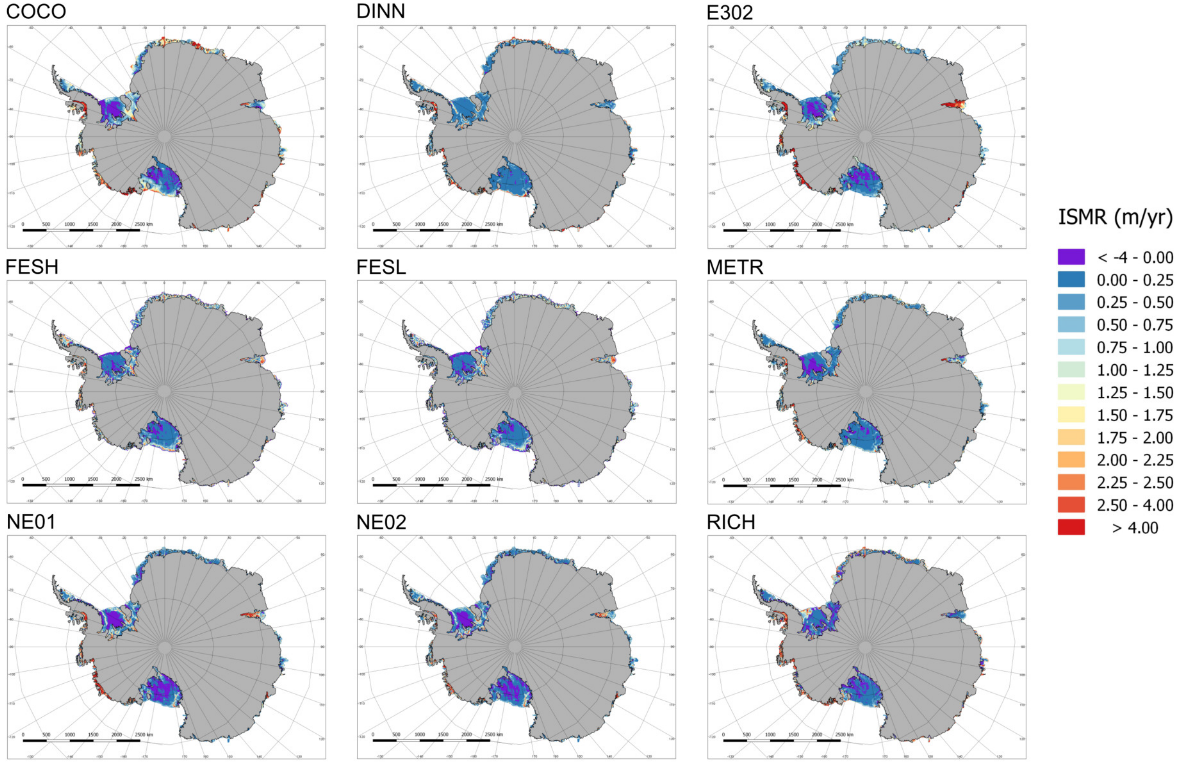

Figure S17. Melt rates, m (m year^{-1}), across all models.

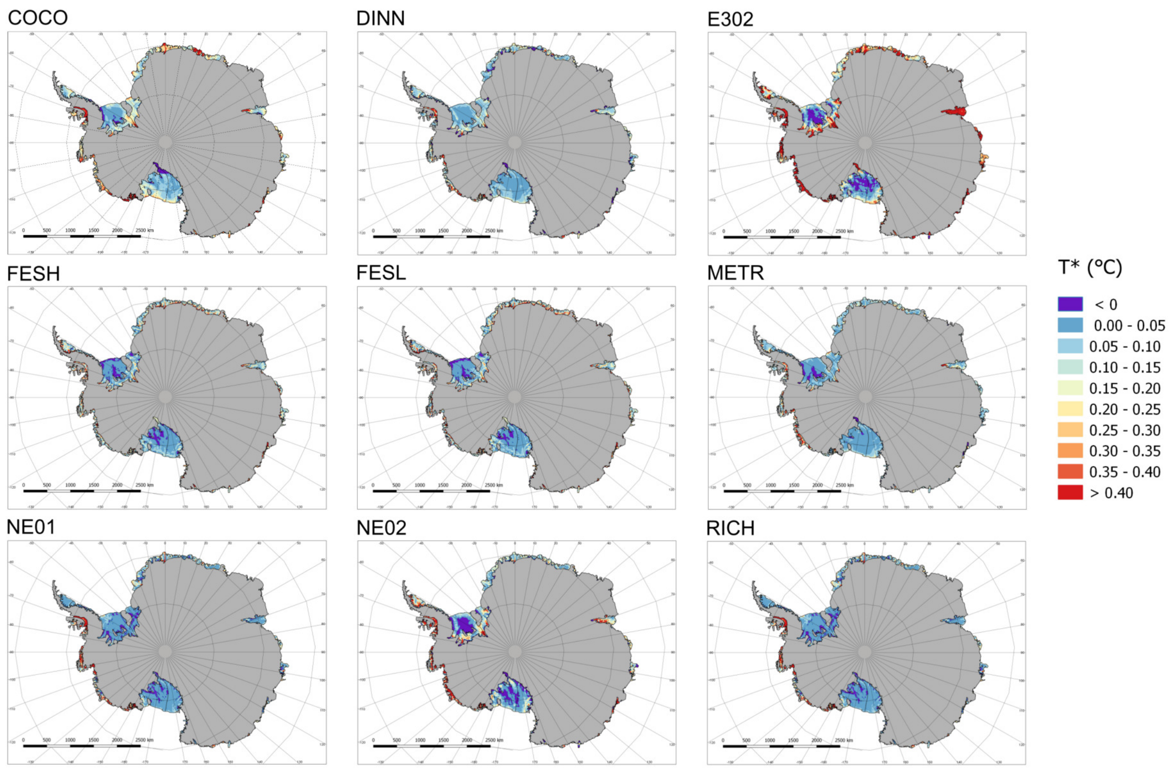

Figure S18. Thermal driving, $T^{\star}$ ($^{\circ}C$), across all models.

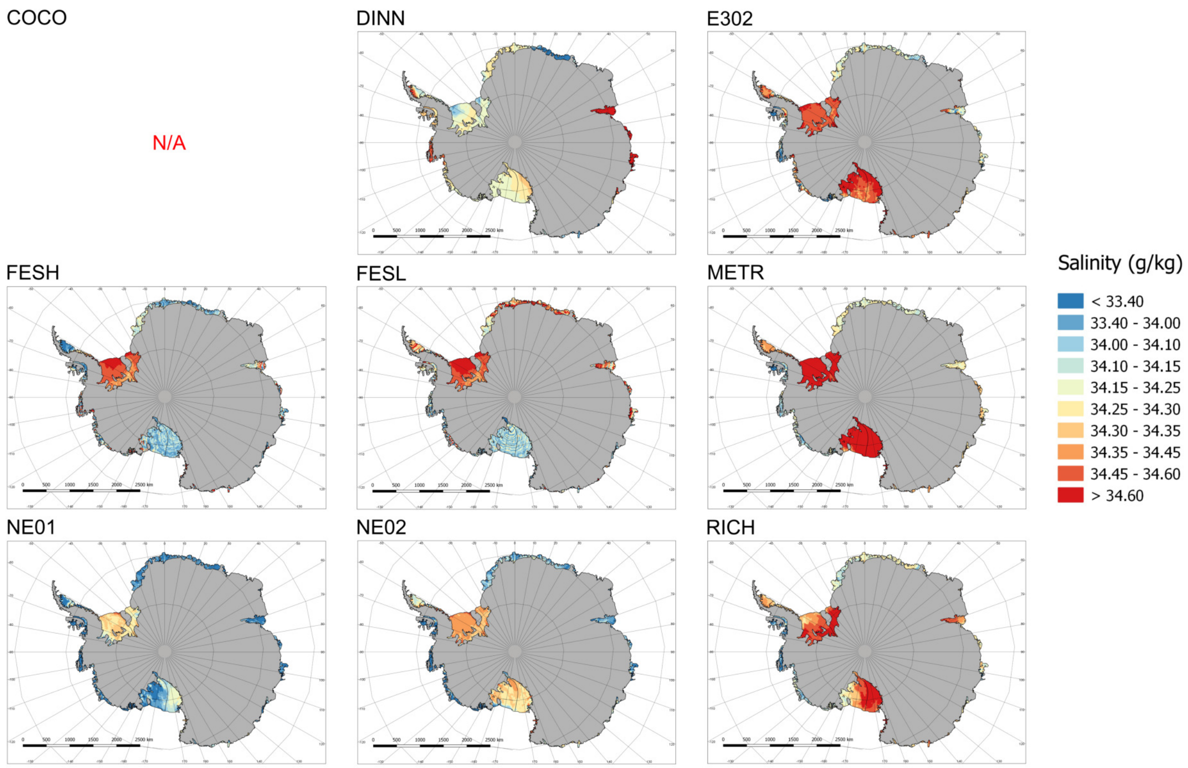

Figure S19. Absolute Salinity at the base of the ice shelf, S_A (g kg^{-1}), across all models.

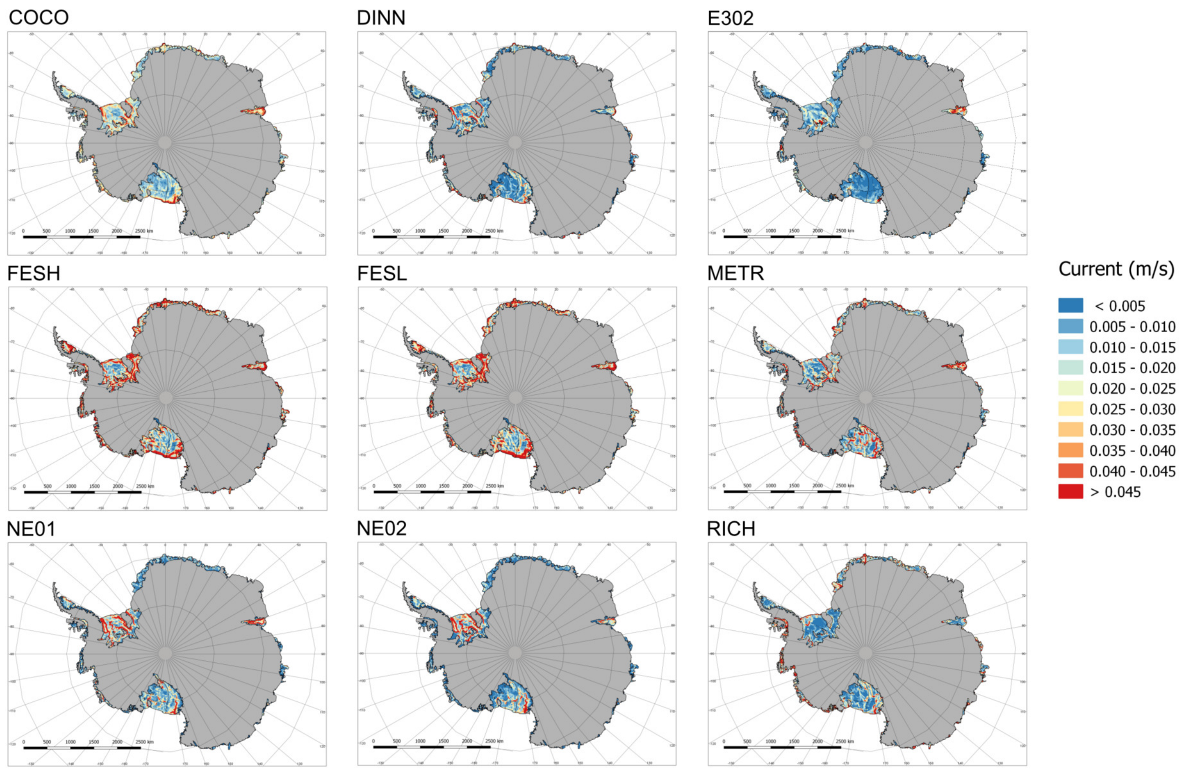

Figure S20. Ocean current speed at the ice shelf base, u_m (m s^{-1}), across all models.

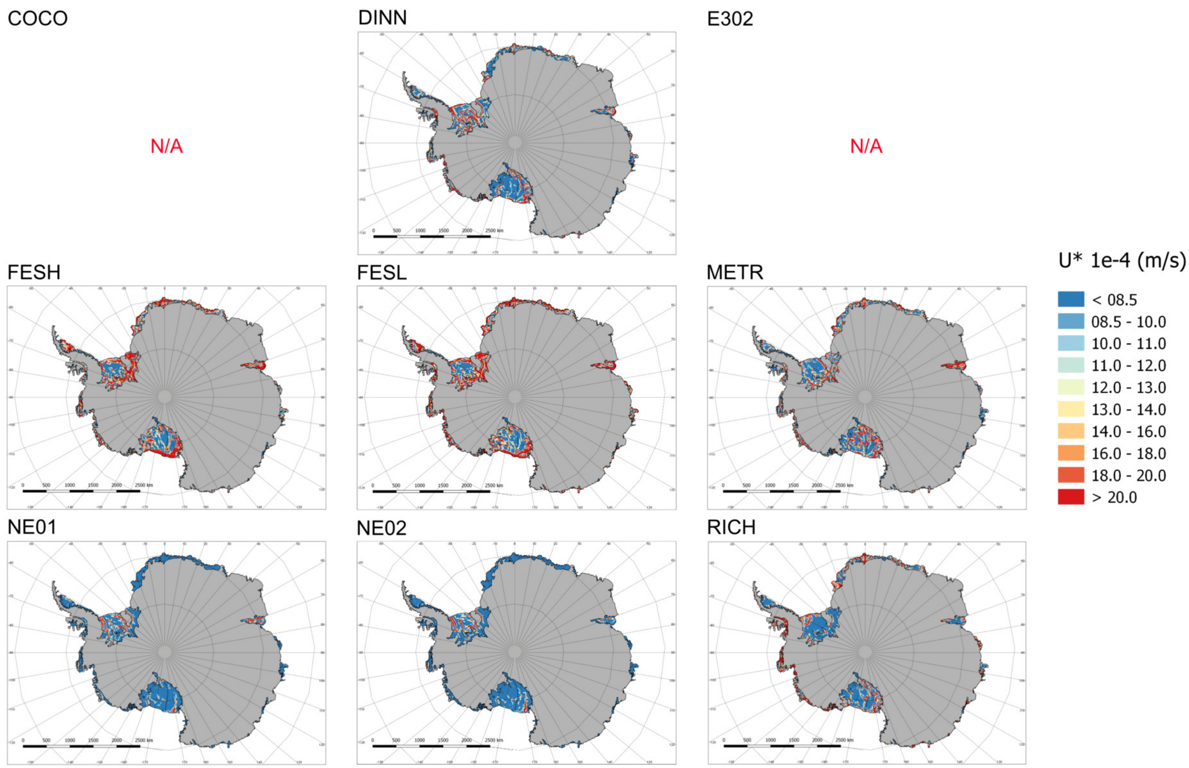

Figure S21. Friction velocity, $u^{\star}$ (m s^{-1}), across all models.

References

Dee, D. P., Uppala, S. M., Simmons, A. J., Berrisford, P., Poli, P., Kobayashi, S., Andrae, U., Balmaseda, M., Balsamo, G., Bauer, d. P., et al.: The ERA-Interim reanalysis: Configuration and performance of the data assimilation system, Quarterly Journal of the royal meteorological society, 137, 553–597, 2011.

Fretwell, P., Pritchard, H. D., Vaughan, D. G., Bamber, J. L., Barrand, N. E., Bell, R., Bianchi, C., Bingham, R., Blankenship, D. D., Casassa, G., et al.: Bedmap2: improved ice bed, surface and thickness datasets for Antarctica, The cryosphere, 7, 375–393, 2013.

Gwyther, D. E., Kusahara, K., Asay-Davis, X. S., Dinniman, M. S., and Galton-Fenzi, B. K.: Vertical processes and resolution impact ice shelf basal melting: A multi-model study, Ocean Modelling, 147, 101 569, 2020.

Losch, M.: Modeling ice shelf cavities in az coordinate ocean general circulation model, Journal of Geophysical Research: Oceans, 113, 2008.

Mathiot, P., Jenkins, A., Harris, C., and Madec, G.: Explicit representation and parametrised impacts of under ice shelf seas in the z^* coordinate ocean model NEMO 3.6, Geoscientific Model Development, 10, 2849–2874, https://doi.org/10.5194/gmd-10-2849-2017, 2017.

Millan, R., Rignot, E., Bernier, V., Morlighem, M., and Dutrieux, P.: Bathymetry of the Amundsen Sea Embayment sector of West Antarctica from Operation IceBridge gravity and other data, Geophysical Research Letters, 44, 1360–1368, 2017.

Morlighem, M., Rignot, E., Binder, T., Blankenship, D., Drews, R., Eagles, G., Eisen, O., Ferraccioli, F., Forsberg, R., Fretwell, P., et al.: Deep glacial troughs and stabilizing ridges unveiled beneath the margins of the Antarctic ice sheet, Nature geoscience, 13, 132–137, 2020.

Pelletier, C., Fichefet, T., Goosse, H., Haubner, K., Helsen, S., Huot, P.-V., Kittel, C., Klein, F., Le clec'h, S., van Lipzig, N. P. M., Marchi, S., Massonnet, F., Mathiot, P., Moravveji, E., Moreno-Chamarro, E., Ortega, P., Pattyn, F., Souverijns, N., Van Achter, G., Vanden Broucke, S., Vanhulle, A., Verfaillie, D., and Zipf, L.: PARASO, a circum-Antarctic fully coupled ice-sheet–ocean–sea-ice–atmosphere–land model involving f.ETISh1.7, NEMO3.6, LIM3.6, COSMO5.0 and CLM4.5, Geoscientific Model Development, 15, 553–594, https://doi.org/10.5194/gmd-15-553-2022, 2022.

Schaffer, J., Timmermann, R., Arndt, J. E., Kristensen, S. S., Mayer, C., Morlighem, M., and Steinhage, D.: A global, high-resolution data set of ice sheet topography, cavity geometry, and ocean bathymetry, Earth System Science Data, 8, 543–557, https://doi.org/10.5194/essd-8-543-2016, 2016.

Tamura, T., Ohshima, K. I., Nihashi, S., and Hasumi, H.: Estimation of Surface Heat/Salt Fluxes Associated with Sea Ice Growth/Melt in the Southern Ocean, SOLA, 7, 17–20, https://doi.org/10.2151/sola.2011-005, 2011.

Timmermann, R., Le Brocq, A., Deen, T., Domack, E., Dutrieux, P., Galton-Fenzi, B., Hellmer, H., Humbert, A., Jansen, D., Jenkins, A., Lambrecht, A., Makinson, K., Niederjasper, F., Nitsche, F., Nøst, O. A., Smedsrud, L. H., and Smith, W. H. F.: A consistent data set of Antarctic ice sheet topography, cavity geometry, and global bathymetry, Earth System Science Data, 2, 261–273, https://doi.org/10.5194/essd-2-261-2010, 2010.